28 P

N64-24105

TECHNICAL MEMORANDUM

Code 1 Cat. 24
NASA TMX 52033

MONTE CARLO SOLUTION FOR THE CHARACTERISTICS OF A HIGHLY RAREFIED IONIZED GAS FLOWING THROUGH A CHANNEL WITH A TRANSVERSE MAGNETIC FIELD

by Morris Perlmutter
Lewis Research Center
Cleveland, Ohio

TECHNICAL PREPRINT prepared for

Fourth International Symposium on Rarefied Gas Dynamics sponsored by the Air Force Office of Scientific Research, the National Aeronautics and Space Administration, the Office of Naval Research, and the University of Toronto
Toronto, Canada, July 7-14, 1964

NATIONAL AERONAUTICS AND SPACE ADMINISTRATION

MONTE CARLO SOLUTION FOR THE CHARACTERISTICS OF A HIGHLY RAREFIED IONIZED GAS FLOWING THROUGH A CHANNEL WITH A TRANSVERSE MAGNETIC FIELD

by Morris Perlmutter

Lewis Research Center

National Aeronautics and Space Administration

Cleveland, Ohio

ABSTRACT

24105

The steady flow of a highly rarefied ionized gas through a channel with a magnetic field normal to the channel wall is studied. The solution is obtained by a Monte Carlo procedure. This method consists of following sample ions through the channel. By tallying properties of these ions as they pass scoring cross sections of the channel, the various local properties of the flows such as density, mass flows, energies, and wall shear stress are obtained. These results for the small magnetic field cases were compared with the limiting analytical solutions for no magnetic field and were in good agreement with them.

Author

I. INTRODUCTION

The equations to be solved for the flow of a fully ionized collisionless rarefied gas through a channel are complex and not readily solvable by the usual analytical procedures, Pai (1962). The Monte Carlo procedure was used in the present case to obtain the various flow characteristics and to give an insight into the behavior of the flow of a collisionless rarefied fully ionized gas through a flat plate channel. These solutions can be used for comparison with other techniques and also to illustrate the use of the Monte Carlo technique for similar types of problems.

The present model consists of a finite length channel of infinite depth as shown in Fig. 1. There is a uniform magnetic field B_2 normal to the channel wall. The left and right end of the channel are open to reservoirs

containing a fully ionized gas in a Maxwellian distribution of velocities at the same temperatures but different densities and pressures. The mean free path in the gas is considered large compared with the dimensions of the channel so that interionic collision effects can be neglected in the channel. The only collisions inside the channel will be by the ions with the walls. The ions are assumed to be reflected from the walls diffusely with a velocity distribution based on the temperature of the wall. It is assumed that the wall is at the same temperature as the reservoirs. The electrical charge of the molecule is assumed unchanged by the wall reflection. Other conditions can be readily assumed using a similar Monte Carlo procedure. The ionized gas can be considered to be composed of positive, negative, and neutral molecules. In the present model each specie can be treated independently since the interaction between them is considered negligible, then these solutions can be summed to give the overall results.

The Monte Carlo procedure consists of following the probable history of a sample charged ion through the channel. By use of a high-speed electronic computor a large number of these sample histories can be carried out in a short time and from these the desired mean quantities are obtained. This method follows the techniques used in solving thermal radiation problems by Monte Carlo as described by Howell and Perlmutter (1963).

The mass through-flow profile and transverse mass flow, the local density, and temperatures as well as the wall shear stress distribution are given. These results are obtained by scoring various properties of the molecules as they pass different cross sections of the channel. The solution for the case of neutral molecules or the case of negligible magnetic field has been obtained analytically by Perlmutter (1964) and is used as a limiting case check on the Monte Carlo results.

II. HISTORY OF SAMPLE ION

The model (Fig. 1) consists of two plates whose length divided by the channel height is l. The plates are infinite in depth. There is a magnetic field of strength B_2 normal to the plates. The gas in the left reservoir has a density ρ_L while the right reservoir is at ρ_R. The molecules are of mass M and charge e. All of the sample ion histories begin at the channel entrance $x_1 = 0$. The number of molecules C_L that each sample molecule entering from the left reservoir represents is given by

$$C_L = \frac{m_L}{MN_L} \tag{1}$$

where m_L is the mass flow rate per unit area, $m_L = \rho_L/2\pi^{1/2}\beta$, entering the channel (Kennard (1939)), N_L is the number of trial molecules used per unit entrance area per unit time.

The Monte Carlo flow chart used in the present calculations is shown in Fig. 2. The position x_{2i} representing the height at which the sample ion enters the channel is given by R, where R is a randomly chosen number between 0 and 1. This is because the molecules are equally likely to enter the channel at any value of x_2. The magnitude of the speed of the sample ion V_i, and the angles ψ and θ which determine its direction, as derived in the appendix A (Eq. (A5) or (A9)), can be obtained from

$$R_v = \left(1 + \frac{v^2}{r_a^2}\right)e^{-v^2/r_a^2} \qquad \text{or} \qquad \frac{v^2}{r_a^2} = -\ln(R_1 R_r) \tag{2a}$$

$$R_\theta = \frac{\theta}{2\pi} \tag{2b}$$

$$R_\psi = \sin^2\psi \tag{2c}$$

where each R represents a new random number, v is the dimensionless velocity given in the nomenclature and ranges from 0 to ∞, ψ is the cone angle from 0 to $\pi/2$, and θ is the polar angle from 0 to 2π. Then the initial

components of velocity of the sample molecule that enters the channel from the left reservoir are

$$v_{1L} = v \cos \psi \tag{3a}$$

$$v_{2L} = v \sin \psi \sin \theta \tag{3b}$$

$$v_{3L} = v \sin \psi \cos \theta \tag{3c}$$

By choosing random numbers between 0 and 1, we can obtain a velocity and direction for the molecule entering the channel that, when taken over a large number of trials, will satisfy the correct theoretical distribution as given in Eq. (A3). These velocities are determined at ⟨1⟩ in the flow chart, where ⟨ ⟩ refers to a particular location in the flow chart. After the ions enter the channel, their behavior will be determined by the relations (Patterson (1962))

$$\frac{dv_1}{d\tau} = -v_3 \tag{4a}$$

$$\frac{dv_2}{d\tau} = 0 \tag{4b}$$

$$\frac{dv_3}{d\tau} = v_1 \tag{4c}$$

which are the equations of motion for an ion through a magnetic field. The τ is the nondimensional time given in the nomenclature. These equations can be solved to give the velocity components as a function of time

$$v_1 = v_{1i} \cos \tau - v_{3i} \sin \tau \tag{5a}$$

$$v_2 = v_{2i} \tag{5b}$$

$$v_3 = v_{1i} \sin \tau + v_{3i} \cos \tau \tag{5c}$$

where the subscript i refers to time $\tau = 0$.

The positions of the molecule as a function of time can be obtained from

$$(x_1 - x_{1i}) = v_{1i} \sin \tau + v_{3i}(\cos \tau - 1) \tag{6a}$$

$$(x_2 - x_{2i}) = v_{2i}\tau \tag{6b}$$

$$(x_3 - x_{3i}) = v_{3i} \sin \tau + v_{1i}(1 - \cos \tau) \tag{6c}$$

The ion will travel in a helical path that is circular in the x_1,x_3-plane and will move with a constant component of velocity in the $\pm x_2$-direction. The radius of the circular ion path in the x_1,x_3-plane, called the gyromagnetic radius, divided by the distance between the plates is

$$\left(v_{1i}^2 + v_{3i}^2\right)^{1/2} \tag{7}$$

The average gyromagnetic radius divided by the width of the channel for all the molecules based on conditions in the left reservoir is

$$r_a = \left(\overline{v_{1L}^2} + \overline{v_{3L}^2}\right)^{1/2} = \frac{1}{\beta D \omega} \tag{8}$$

which is equal to the Larmor radius divided by the width of the channel. The term $\overline{v_{1L}^2}$ is equal to $\int v_{1L}^2 f_M \, d^3v$. The details of the remaining history of the ion is given in appendix B. The ion is followed through the channel until it leaves from either end and then a new ion is started. This is continued until a preset number of histories are carried out.

III. MEAN FLOW VALUES FROM SAMPLE HISTORIES

A. Transport of Some Ion Property Q in Channel

At some point along the channel length $x_1 = \mathfrak{L}$, the channel height is divided into increments of width Δx_2. In the present case 20 increments across the channel height were used. Increment p is given by $p = (x_2/\Delta x_2)_{\text{integer}} + 1$. The net amount of Q that is being carried across the incremental area Δx_2 is then given by

$$\frac{C_L\left(\sum^{S^+} Q - \sum^{S^-} Q\right)_{L,\mathfrak{L},p}}{D\,\Delta x_2} + \frac{C_R\left(\sum^{S^+} Q - \sum^{S^-} Q\right)_{R,\mathfrak{L},p}}{D\,\Delta x_2} = \frac{\rho \overline{V_1 Q}}{M} = \int Q V_1 f \, d^3V \tag{9}$$

where the subscripts L and R denote the sample molecule origin in the left or right reservoir. The terms S^+ and S^- are the number of sample

molecules passing through the increment in the positive or negative x_1 directions, respectively. Substituting from the definition of C from Eq. (1) we obtain

$$\frac{m_L}{D\,\Delta x_2}\frac{\left(\sum^{S^+} Q - \sum^{S^-} Q\right)_{L,\mathfrak{L},p}}{N_{R_L}} + \frac{m_R}{D\,\Delta x_2}\frac{\left(\sum^{S^+} Q - \sum^{S^-} Q\right)_{R,\mathfrak{L},p}}{N_R} = \rho\overline{V_1 Q} \quad (10)$$

When $m_L = m_R$, $\rho\overline{V_1 Q} = \rho\overline{V_1 Q}_{m_L=m_R}$. Subtracting this from Eq. (10) gives

$$\frac{\left(\sum^{S^+} Q - \sum^{S^-} Q\right)_{L,\mathfrak{L},p}}{D\,\Delta x_2 N_L} = \frac{\rho\overline{V_1 Q} - \rho\overline{V_1 Q}_{m_L=m_R}}{m_L - m_R} \quad (11)$$

The above operation is possible because there is no interaction between the molecules and therefore $\left[\left(\sum^{S^+} Q - \sum^{S^-} Q\right)_{L,\mathfrak{L},p}\right]\Big/(N_L D\,\Delta x_2)$ is independent of m_L. A similar relation holds for the sample ions entering from the right reservoir.

1. Mass flow profile through channel. - Since the local mass flow through the channel is given by $\rho u_1 = M\int V_1 f\, d^3V$, Q in Eq. (10) for this case is 1. The u_1 is the local mean through-flow velocity in the x_1-direction and is equal to $\int V_1 f\, d^3V$. The numerical calculations showed that the results for $\left[(S^+ - S^-)_{L,\mathfrak{L},p}\right]/(N_L D\,\Delta x_2)$ were equal at x_1 and $l - x_1$. By symmetry $\left[(S^+ - S^-)_{L,x_1,p}\right]/(N_L D\,\Delta x_2)$ is equal to $\left[-(S^+ - S^-)_{R,l-x_1,p}\right]/(N_R D\,\Delta x_2)$. Using these relations in Eq. (10) gives

$$\frac{\rho u_1}{m_L - m_R} = \frac{(S^+ - S^-)_{L,\mathfrak{L},p}}{N_L D\,\Delta x_2} \quad (12)$$

Relating this to Eq. (11) shows that $\rho u_{1_{m_L=m_R}} = 0$, that is, when the two reservoirs are at the same condition there is no net through-flow anywhere in the channel. Equation (12) shows that, for this case, it is only necessary to consider the sample molecules originating in the left reservoir to obtain the complete solution. The axial mass profile results are shown in Fig. 3.

The curves are symmetric between the upper and lower halves of the channel $(\rho u_1)_{x_2} = (\rho u_1)_{l-x_2}$ and also symmetric around the front and back ends of the channel $(\rho u_1)_{x_1} = (\rho u_1)_{l-x_1}$.

The solid line, which is the analytical solution for $r_a = \infty$ (Perlmutter, (1964)) is in good agreement with the Monte Carlo results for r_a of 1000. Thus, for this value of r_a the solution is close to the limiting case for no magnetic field for this range of l's. Also the fact that the results are in agreement for the two different methods indicates the validity of the Monte Carlo procedure.

The average mass flow through the channel can be obtained from Eq. (12) by summing the results for each increment and then dividing by the number of increments:

$$\frac{(\rho u_1)_{av}}{m_L - m_R} = \left(\frac{\sum^{l/\Delta x_2} S^+}{DN_L} \right)_{L,l,p} \tag{13}$$

where $(S^+)_{L,l,p}$ is the total number of trial molecules leaving the right end of the channel through the increment Δx_2. These results are shown in Fig. 4. It can be seen that as r_a decreases, the mass flow through the channel decreases. This is true because, for small values of r_a, the charged molecules are trapped to rotate in small circular orbits around the magnetic lines of force.

2. Transverse mass flow. - The flow in the x_3 or depth direction is given by $\rho u_3 = M \int_0^\infty V_3 f \, dV$; then in Eq. (10) for this case $Q = V_3/V_1$. The numerical calculations showed that the results for

$$\frac{\left[\sum^{S^+} \left(\frac{v_3}{v_1} \right) - \sum^{S^-} \left(\frac{v_3}{v_1} \right) \right]_{L,\ell,p}}{N_L D \, \Delta x_2} \tag{14}$$

were the same at x_1 and $l - x_1$. Following the same procedure as followed before, $(\rho u_3)_{m_L = m_R} = 0$, and we obtain

$$\frac{\rho u_3}{m_L - m_R} = \frac{\left[\sum^{S^+}\left(\frac{v_3}{v_1}\right) - \sum^{S^-}\left(\frac{v_3}{v_1}\right)\right]_{L,\mathfrak{L},p}}{N_L D\,\Delta x_2} \tag{15}$$

As for ρu_1, the flow ρu_3 is symmetric around the midplane parallel to the channel walls $\rho u_{3,x_2} = \rho u_{3,1-x_2}$ and it is also symmetrical around the midplane between the front and rear ends of the channel, $\rho u_{3,x_1} = \rho u_{3,l-x_1}$.

The average transverse flow through the channel can then be obtained by summing the flow across the channel and dividing by the channel height:

$$\frac{(\rho u_3)_{av}}{m_L - m_R} = \frac{\sum^{1/\Delta x_2}\left[\sum^{S^+}\left(\frac{v_3}{v_1}\right) - \sum^{S^-}\left(\frac{v_3}{v_1}\right)\right]_{L,\mathfrak{L},p}}{N_L D} \tag{16}$$

These results are shown in Fig. 5. When there is no magnetic field $1/r_a = 0$ the transverse flow is zero. The transverse flow begins to decrease for large values of $1/r_a$ corresponding to large magnetic fields. This is true because the molecules are making orbits of very small radii around the magnetic lines of force, thereby preventing any large mass flows. The results indicate that the maximum value of the transverse flow occurs in the middle of the channel for values of r_a of approximately half the channel length. The largest transverse flows occur in the smallest length channels, $l = 0.1$.

3. Density profile. - The local density is given by $\rho = M \int f\, dV$. Then $Q = 1/V_1$ in Eq. (10). The numerical calculations obeyed the relation

$$\frac{\left(\sum^{S^+}\frac{1}{v_1} - \sum^{S^-}\frac{1}{v_1}\right)_{L,x_1,p}}{D\,\Delta x_2 N_L 2\sqrt{\pi}\, r_a^{-1}} + \frac{\left(\sum^{S^+}\frac{1}{v_1} - \sum^{S^+}\frac{1}{v_1}\right)_{L,l-x_1,p}}{D\,\Delta x_2 N_L 2\sqrt{\pi}\, r_a^{-1}} = 1 \tag{17}$$

Then from symmetry

$$\frac{\left(\sum^{S^+}\frac{1}{v_1}-\sum^{S^-}\frac{1}{v_1}\right)_{L,x_1,p}}{D\,\Delta x_2 N_L 2\sqrt{\pi}\,r_a^{-1}}=\frac{\left(\sum^{S^+}\frac{1}{v_1}-\sum^{S^-}\frac{1}{v_1}\right)_{R,l-x_1,p}}{D\,\Delta x_2 N_R 2\sqrt{\pi}\,r_a^{-1}} \tag{18}$$

Following the same procedure as before, we find that $\rho_{m_L=m_R}=\rho_R$, and we obtain

$$\frac{\rho-\rho_R}{\rho_L-\rho_R}=\frac{\left(\sum^{S^+}\frac{1}{v_1}-\sum^{S^-}\frac{1}{v_1}\right)_{L,\mathfrak{L},p}}{D\,\Delta x_2 N_L 2\sqrt{\pi}\,r_a^{-1}} \tag{19}$$

These results are shown in Fig. 6. The limiting solution of zero magnetic field agreed well with the Monte Carlo solution for $r_a = 1000$. As r_a becomes smaller, the densities in the channel near the reservoirs approach the density of the reservoir more closely. The densities are symmetrical around the midplane $x_2 = l/2$

$$\left(\frac{\rho-\rho_R}{\rho_L-\rho_R}\right)_{x_2}=\left(\frac{\rho-\rho_R}{\rho_L-\rho_R}\right)_{l-x_2} \tag{20}$$

and are related around the midplane $x_1 = l/2$ by

$$\left(\frac{\rho-\rho_R}{\rho_L-\rho_R}\right)_{x_1}+\left(\frac{\rho-\rho_R}{\rho_L-\rho_R}\right)_{l-x_1}=1 \tag{21}$$

4. Local kinetic energy. - The kinetic energy at some location is given by $\rho E = (M/2)\int V^2 f\,dV$. Then Q in Eq. (10) for this case is $V^2/2V_1$. The numerical calculations obeyed the relation

$$\frac{\left[\sum^{S^+}\left(\frac{v^2}{v_1}\right)-\sum^{S^-}\left(\frac{v^2}{v_1}\right)\right]_{L,x_1,p}}{3\sqrt{\pi}\,D\,\Delta x_2 N_L r_a}+\frac{\left[\sum^{S^+}\left(\frac{v^2}{v_1}\right)-\sum^{S^-}\left(\frac{v^2}{v_1}\right)\right]_{L,l-x_1,p}}{3\sqrt{\pi}D\,\Delta x_2 N_L r_a}=1 \tag{22}$$

Then following the same procedure as before we find that $(\rho E)_{m_L=m_R}=3\rho_R/4\beta^4$, which is the kinetic energy in the reservoir (Perlmutter (1964)) and the solution reduces to

$$\frac{\frac{4\beta^2}{3}(\rho E) - \rho_R}{\rho_L - \rho_R} = \frac{\left[\sum^{S^+}\left(\frac{v^2}{v_1}\right) - \sum^{S^-}\left(\frac{v^2}{v_1}\right)\right]}{3\sqrt{\pi}\, D\, \Delta x_2 N_L r_a}\; L,\mathfrak{L},p \tag{23a}$$

Again there is symmetry around the midplane $x_2 = 1/2$ of the channel,

$$\left[\frac{\frac{4\beta^2}{3}(\rho E) - \rho_R}{\rho_L - \rho_R}\right]_{x_2} = \left[\frac{\frac{4\beta^2}{3}(\rho E) - \rho_R}{\rho_L - \rho_R}\right]_{1-x_2} \tag{24}$$

while around the plane $x_1 = l/2$ of the channel,

$$\left[\frac{\frac{4\beta^2}{3}(\rho E) - \rho_R}{\rho_L - \rho_R}\right]_{x_1} + \left[\frac{\frac{4\beta^2}{3}(\rho E) - \rho_R}{\rho_L - \rho_R}\right]_{l-x_1} = 1 \tag{25}$$

For zero magnetic field (Perlmutter (1964)) it was shown that $(\rho E)_{r_a=\infty} = 3\rho/4\beta^2$. For this case

$$\left[\frac{\frac{4\beta^2}{3}(\rho E) - \rho_R}{\rho_L - \rho_R}\right]_{r_a=\infty} = \left(\frac{\rho - \rho_R}{\rho_L - \rho_R}\right)_{r_a=\infty} \tag{23b}$$

The results plotted in Fig. 6 show that for smaller values of r_a the value of $(4\beta^2/3)(\rho E)$ is no longer equal to ρ as for the nonmagnetic case, but has decreased near the entrance of the channel and increased near the exit. This is true because the higher velocity molecules have a larger gyromagnetic radius and so diffuse more readily down the channel than the slower moving molecules.

B. Collision Rate With Walls

The mass flow rate incident per unit area on the upper wall and then reflected can be obtained as follows: The channel wall is divided into increments of width Δx_1. In the present calculations, 20 increments along the channel surface were used. At a particular increment q, given by $q = (x_1/\Delta x_1)_{\text{integer}} + 1$, the number of sample molecules colliding into this

increment is scored:

$$\frac{C_L(S_q)_L}{D\,\Delta x_1} + \frac{C_R(S_q)_R}{D\,\Delta x_1} = \frac{1}{M}\,m_w = \int_{\Omega} V_2 f\,dV \tag{26}$$

This can be rewritten as

$$m_w = \frac{m_L}{N_L D\,\Delta x_1}(S_q)_L + \frac{m_R(S_q)_R}{N_R D\,\Delta x_1} \tag{27}$$

From the numerical calculations it was noted that

$$\frac{(S_{L,q})_{x_1}}{N_L D\,\Delta x_1} + \frac{(S_{L,q})_{l-x_1}}{N_L D\,\Delta x_1} = 1 \tag{28}$$

Since by symmetry

$$\frac{(S_{L,q})_{l-x_1}}{N_L D\,\Delta x_1} = \frac{(S_{R,q})_{x_1}}{N_R D\,\Delta x_1} \tag{29}$$

we find that $(m_w)_{m_L=m_R} = m_R$ and Eq. (26) becomes

$$\frac{m_w - m_R}{m_L - m_R} = \frac{(S_q)_L}{N_L D\,\Delta x_1} \tag{30}$$

These results are shown in Fig. 7. Again there is good agreement between the limiting analytical solution for $r_a = \infty$ and the Monte Carlo solution for $r_a = 1000$. For the smaller values of r_a the mass flow reflected from the wall near the reservoir is closer to the mass flow into the reservoir. These results are the same for the upper and lower wall and are related around the channel midplane $x_1 = l/2$ by

$$\left(\frac{m_w - m_R}{m_L - m_R}\right)_{x_1} + \left(\frac{m_w - m_R}{m_L - m_R}\right)_{l-x_1} = 1 \tag{31}$$

C. Shear Stress at Wall

The shear stress on the surface in the x_1-direction is given by $p_{x_1,x_2} = (-\rho V_1' V_2')_w$, where V' is the random component of velocity $V = V' + u$, where $\int V' f\,d^3V = 0$. Since u_2 at the wall is zero then $(-\rho\overline{V_1' V_2'})_w$ is equal to $(-\rho\overline{V_1 V_2})_w$. Since the ions are reflected diffusely they do not contribute

to the surface shear so we obtain

$$\left(\frac{\rho\overline{V_1'V_2'}}{M}\right)_w = \left(\int_\Omega V_1 V_2 f \, dV\right)_w = \frac{C_L\left(\sum^{S_q} V_1\right)_L}{D\,\Delta x_1} + \frac{C_R\left(\sum^{S_q} V_1\right)_R}{D\,\Delta x_1} \tag{32}$$

As before, from the numerical calculations,

$$\frac{\left(\sum^{S_q} V_1\right)_{L,x_1}}{D\,\Delta x_1 N_L} = \frac{\left(\sum^{S_q} V_1\right)_{L,l-x_1}}{D\,\Delta x_1 N_L} \tag{33}$$

and proceeding in a similar manner, we find $(\rho\overline{V_1V_2})_{w,m_L=m_R} = 0$ and obtain from Eq. (32)

$$\frac{\left(\rho\overline{V_1'V_2'}\right)_w}{\left(\frac{m_L^2}{\rho_L} - \frac{m_R^2}{\rho_R}\right)} = \frac{\left(\sum^{S_q} V_1\right)_L}{\Delta x_1 N_L D r_a (2\pi^{1/2})^{-1}} \tag{34}$$

These results are shown in Fig. 8 and are the same on the upper and lower walls. The results are also symmetrical around $x_1/l = 0.5$. The shear stress for r_a of 1000 is seen to agree well with the nonmagnetic analytical solution. The shear stress is seen to decrease for smaller values of r_a. Since this corresponds to smaller values of mass flow through the channel, this result would be expected.

IV. CONCLUSIONS

The effect of the increasing magnetic field is to reduce the mass flow of the ions through the channel. The magnetic field also causes a transverse mass ion flow to occur perpendicular to the through-flow and parallel to the channel walls. This transverse flow reaches a maximum and then decreases as the magnetic field becomes stronger. The decrease is due to the strong magnetic field trapping the charged particles.

The Monte Carlo solution worked well with this problem. The major drawback was the large amount of computer time necessary to run the analysis. Generally, 200,000 sample ions were needed for each case to reduce the scatter in the results. A lesser number of trials gave points falling around the correct solution but with larger scatter. The trials were run on an IBM 7094 computer and each case ran approximately 45 minutes. The amount of time each sample ion ran would increase with longer channels and higher magnetic fields. The scatter is decreased if a large number of sample ions are tallied at a particular position so that more meaningful statistical averages can be obtained. More advanced techniques, such as splitting or Russian roulette, could be used to decrease the computing time. With this Monte Carlo procedure, other boundary conditions can readily be used and the method could be extended to include interionic collisions.

APPENDIX A - ENTERING ION SPEED AND DIRECTION

The number of molecules moving in the x_1-direction $f_M^+ \, d^3V$, where $d^3V = dV_1 \, dV_2 \, dV_3$, with the velocity in the range d^3V for an assumed Maxwellian distribution, is given by

$$f_M^+ \, d^3V = \frac{\rho_L \beta^3}{\pi^{3/2} M} e^{-\beta^2 V^2} \, dV_1 \, dV_2 \, dV_3 \tag{A1}$$

where $V^2 = V_1^2 + V_2^2 + V_3^2$. The number of molecules entering the channel per unit time per unit area in the incremental velocity range of d^3V from the left reservoir is given by $dm_L/M = V_1 f_M^+ \, d^3V$. If this is integrated over V_1 from 0 to ∞, V_2 and V_3 from $-\infty$ to $+\infty$ we obtain for the total flow entering the channel $m_L = \rho_L/(2\beta\pi^{1/2})$. The distribution of velocities of the ions entering the channel from the left reservoir then can be written as

$$V_1 f_M^+ \, dV = \frac{2\beta^4 m_L}{\pi} V_1 e^{-\beta^2 V^2} \, d^3V \tag{A2}$$

This can be transformed into spherical coordinates where $V_1 = V \cos \psi$;

$V_2 = V \sin\psi \sin\theta$; $V_3 = V \sin\psi \cos\theta$, where ψ is the cone angle measured from the x_1-axis, and θ is the polar angle measured from the x_1, x_3-plane. Then (A2) can be written as

$$\frac{V_1 f_M^+ \, d^3V}{m_L} = \frac{2\beta^4}{\pi} V^3 e^{-\beta^2 V^2} \cos\psi \sin\psi \, d\psi \, d\theta \, dV \tag{A3}$$

This gives the fraction of all the molecules in the ranges $dV \, d\theta \, d\psi$ entering the channel. The fraction of molecules that are in the velocity range dV is given by taking the marginal distribution $f_{M,V}$ which is obtained by integrating (A3) over θ from 0 to 2π and ψ from 0 to $\pi/2$ to give

$$f_{M,V} \, dV = 2\beta^4 V^3 e^{-\beta^2 V^2} \, dV \tag{A4a}$$

Similarly, the marginal frequencies for θ and ψ after integrating over V from 0 to ∞ are

$$f_{M,\theta} \, d\theta = \frac{d\theta}{2\pi} \tag{A4b}$$

$$f_{M,\psi} \, d\psi = 2 \cos\psi \sin\psi \, d\psi \tag{A4c}$$

We can pick from this distribution by setting the random number R equal to the cumulative distribution function, $R = \int_{-\infty}^{x} f_{M_{x'}} \, dx'$ as in Howell and Perlmutter (1963). Then the machine can pick a random number R and solve for the random variable x from the above relation. For Eqs. (A4a), (A4b), and (A4c), this gives

$$R_V = 1 - R_V = (1 + \beta^2 V^2) e^{-\beta^2 V^2} = \left(1 + \frac{v^2}{r_a^2}\right) e^{-v^2/r_a^2} \tag{A5a}$$

$$R_\theta = \frac{\theta}{2\pi} \tag{A5b}$$

$$R_\psi = \sin^2\psi \tag{A5c}$$

Solving for v in Eq. (A5a) for a given R_V is difficult because of its form; however, v could be obtained in the following manner. If Eq. (A2) is written in cylindrical coordinates, we obtain

$$\frac{V_1 f_M^+ \, d^3V}{m_L} = 2\beta^2 V_1 e^{-\beta^2 V_1^2} \, dV_1 \, 2\beta^2 V_r e^{-\beta^2 V_r^2} \, dV_r \, \frac{d\theta}{2\pi} \tag{A6}$$

where $V_1 = V_1$, $V_2 = V_r \cos\theta$ and $V_3 = V_r \sin\theta$. Then as before the new marginal distributions are

$$f_{M,V_1} \, dV_1 = 2\beta^2 V_1 e^{-\beta^2 V_1^2} \, dV_1 \tag{A7a}$$

$$f_{M,V_r} \, dV_r = 2\beta^2 V_r e^{-\beta^2 V_r^2} \, dV_r \tag{A7b}$$

This gives, as before,

$$\beta^2 V_1^2 = -\ln R_1 \tag{A8a}$$

$$\beta^2 V_r^2 = -\ln R_r \tag{A8b}$$

Then

$$\frac{v^2}{r_a^2} = \frac{v_1^2}{r_a^2} + \frac{v_r^2}{r_a^2} = -\ln R_1 - \ln R_r = -\ln R_1 R_r \tag{A9}$$

This means we can pick v by using two random numbers in Eq. (A9).

APPENDIX B - DETAILS OF ION HISTORY

We can define $v_1 = v_R \cos\gamma$ and $v_3 = v_R \sin\gamma$, while $v_{1i} = v_R \cos\gamma_i$ and $v_{3i} = v_R \sin\gamma_i$ (Fig. 9). Substitution into Eq. (5a) or (5c) gives $\tau = \gamma - \gamma_i$. The angle γ can then be calculated from

$$\gamma = \sin^{-1}\left(\frac{v_3}{v_R}\right) \tag{B1}$$

The component of velocity v_2 is unchanged by the magnetic field, and the time at which the sample ion will strike the upper or lower wall after entering the channel is $\tau_w = (1 - x_{2i})/v_{2i}$ or $\tau_w = -x_{2i}/v_{2i}$ (see Fig. 2 ⟨3⟩). Also, the position x_1 at time τ can be determined from Eq. (6a) to be

$$x_1 - x_{1i} = v_R\left[\sin(\tau + \gamma_i) - \sin\gamma_i\right] = v_R \, 2 \sin\frac{\tau}{2} \cos\left(\gamma_i + \frac{\tau}{2}\right) \tag{B2}$$

It is necessary to know the time $\tau_{\mathfrak{L}}$ that a molecule will reach some given position $x_1 = \mathfrak{L}$. This can be obtained from Eqs. (5c) and (6a) since

$$\mathfrak{L} - x_{1i} = v_{3\mathfrak{L}} - v_{3i} \tag{B3}$$

$$v_{1\mathfrak{L}} = \pm\left(v_R^2 - v_{3\mathfrak{L}}^2\right)^{1/2} \tag{B3}$$

where the + and - are used according to the direction the molecule is traveling. Substitution into Eq. (B1) gives $\gamma_{\mathfrak{L}}$, which can be used to find the time, $\tau_{\mathfrak{L}} = \gamma_{\mathfrak{L}} - \gamma_i$. With the time known, the various parameters that are scored can be obtained. From Eq. (6a) evaluated at time τ_w, the position x_{1w} where the molecule strikes the wall is obtained ⟨5⟩.

However, the sample molecule may reach a maximum value of x_1 and then start to circle back before striking the wall. This maximum value of x_1 will occur in this case at $\tau_{max} = \pi/2 - \gamma_i$ (see Fig. 9, ⟨4⟩). Then if τ_{max} is less than τ_w, the molecule will turn before striking the wall, and $x_{1,max}$ is evaluated at τ_{max} ⟨6⟩. If the molecule passes a value of $x_1 = \mathfrak{L}$ ⟨7⟩, its important characteristics are tallied ⟨8⟩. In the present case $\mathfrak{L}$ was taken at 0, $l/4$, $l/2$, $3l/4$, and l. It may pass the exit plane ⟨9⟩ at which point it is tallied and a new molecule is started. If the molecule strikes the wall this is scored in the appropriate wall increment ⟨11⟩, and the molecule is reemitted from this point in a new direction with a new velocity ⟨12⟩. The new direction is picked from a population based on diffuse reflections from the walls, and a new velocity from a population based on a wall temperature which in this case is taken equal to the temperature of the reservoir. This means v, θ, ψ are obtained from Eqs. (2a), (2b), and (2c).

The components of velocity from the lower wall are now given by, ⟨12a⟩

$$\begin{aligned} v_{1\lambda} &= v \sin\psi \sin\theta \\ v_{2\lambda} &= v \cos\psi \\ v_{3\lambda} &= v \sin\psi \cos\theta \end{aligned} \tag{B4}$$

while for the upper walls, ⟨12b⟩

$$v_{1\mu} = v \sin \Psi \sin \theta$$
$$v_{2\mu} = -v \cos \Psi \qquad \text{(B5)}$$
$$v_{3\mu} = v \sin \Psi \cos \theta$$

If the molecule is reflected from the wall with a positive v_1-component, the molecule goes through a similar procedure as just described ⟨13⟩. If the molecule is reemitted with a negative component of v_1 then τ_w is compared with τ_{min}, the time for the molecule to reach its minimum value of x_1. As seen from Fig. 9 this is given by $\tau_{min} = (3\pi/2) - \gamma_i$ ⟨14⟩. Then $x_{1,min}$ is calculated from whichever time is smaller τ_{min} or τ_{wall} ⟨15⟩. Again the pertinent values are scored each time the molecule passes a scoring position $x_1 = \mathfrak{L}$ ⟨16⟩. If the molecule leaves the entrance it is scored ⟨17⟩ and a new molecule is started; however, if it does not leave through the entrance it may hit the wall ⟨11⟩ in which case it is tallied and reemitted as discussed before. If it does not hit the wall or leave the channel, it will start to circle back, and now $\tau_{max} = \tau_{min} + \pi$ (Fig. 9) and the usual procedure continued ⟨19⟩. If it reaches its maximum value of x_1 and does not leave the end of the channel or strike the wall, it will again circle back with $\tau_{min} = \pi + \tau_{max}$ (Fig. 9) and the molecule is followed as before ⟨20⟩. When DN molecules have been followed the results are printed out and the program is stopped ⟨21⟩.

LIST OF SYMBOLS

C number of molecules represented by sample molecule, m/MN

D height of channel

e charge of molecule

f velocity distribution of molecules

f_M Maxwellian velocity distribution

f_M^+ Maxwellian distribution of molecules moving in positive x_1-direction

$\mathfrak{L}$	scoring cross section along x_1
l	length of channel divided by height
M	mass of molecule
m	mass flow rate per unit area
m_L	mass flow in from left reservoir, $\rho_L/(2\pi^{1/2}\beta)$
N	number of trial molecules entering channel per unit time per unit area
n	number of sample molecule
p	pressure
p_{x_1,x_2}	shear stress on surface in x_1-direction
Q	quantity being carried by sample ion
R	random number between 0 and 1
R_g	gas constant
r_a	Larmor radius divided by channel height, $(\beta D\omega)^{-1}$
S	number of molecules passing through increment
T	temperature
u_1,u_2,u_3	components of mean flow
V	molecular velocity
v	dimensionless molecular velocity, $V/D\omega$
v_R	dimensionless velocity in x_1,x_3-plane
x_1,x_2,x_3	coordinates divided by channel height D
z	section of channel
β	parameter $(2RT)^{-1/2}$
γ	angle Eq. (B1)
θ	polar angle
ρ	density
τ	time multiplied by cyclotron frequency ω
ψ	cone angle

ω eB_2/M cyclotron frequency

Subscripts:

i initial time, $\tau = 0$

L left reservoir

$\mathfrak{L}$ location along x_1

M marginal distribution

m Maxwellian

p increment number along x_2

q increment number along x_1

R right reservoir

w wall

λ,μ lower or upper wall, respectively

Ω integration over all velocities in plus x_2-direction

Superscripts:

$(\bar{})$ mean value, $\int ( ) f \, d^3V$

$^+$ in positive x_1-direction

$^-$ in negative x_1-direction

$(')$ undirected component

REFERENCES

Howell, J. R., and Perlmutter, M. (1963). Monte Carlo Solution of Radiant Heat Transfer in a Nongrey Nonisothermal Gas with Temperature Dependent Properties. Paper 6051, (to be published in A.I.Ch.E. Journal).

Kennard, Earl E. (1939). "Kinetic Theory of Gases," McGraw Hill Book Co., Inc.

Pai, S. I. (1962). "Magnetogasdynamics and Plasma Dynamics," Prentice Hall Book Co., Inc.

Patterson, G. N. (1962). "Mechanics of Rarefied Gases and Plasmas," Rev. 18, Inst. Aerophys., Toronto Univ.

Perlmutter, Morris (1964). "Flow and Heat Transfer Between Heated Plates of Finite Width in a Free-Molecule-Flow Environment." Proposed NASA TN.

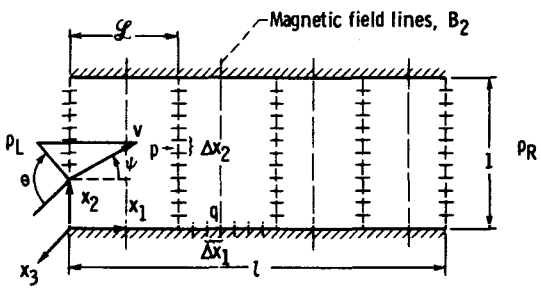

Figure 1. - Model.

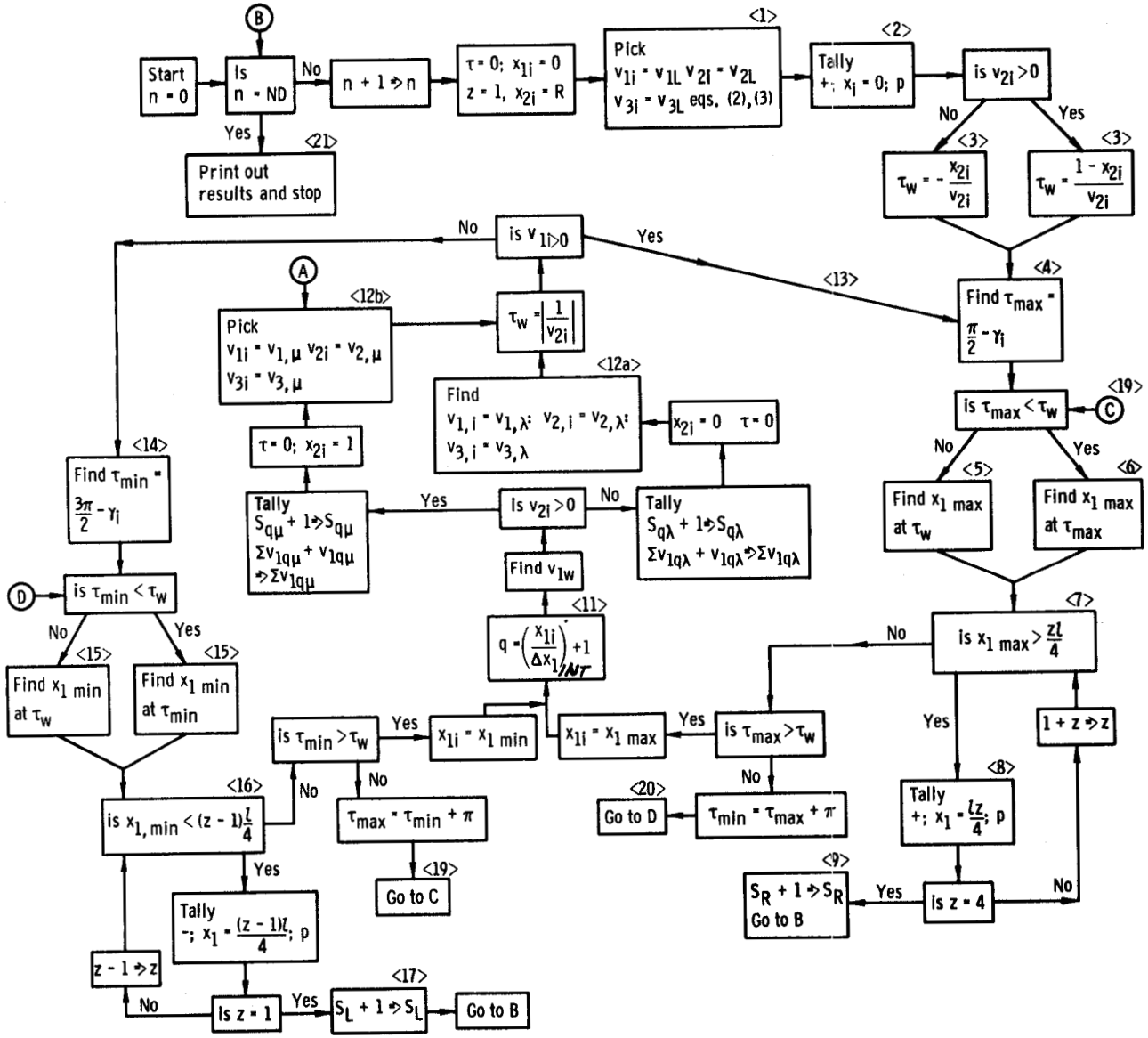

Figure 2. - Monte Carlo flow chart.

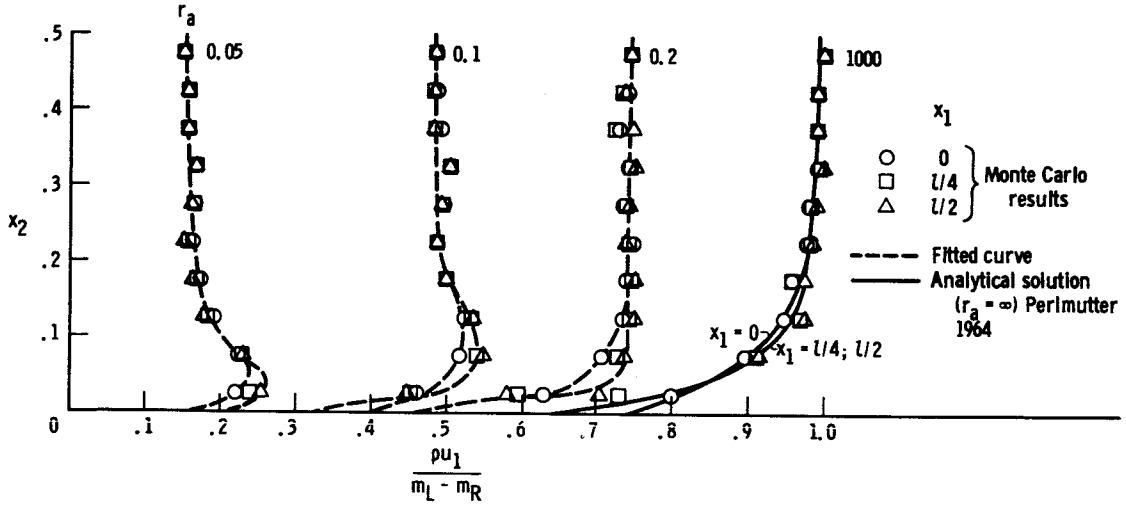

(a) Channel length divided by height, $l = 0.1$.

Figure 3. - Axial mass flow profiles.

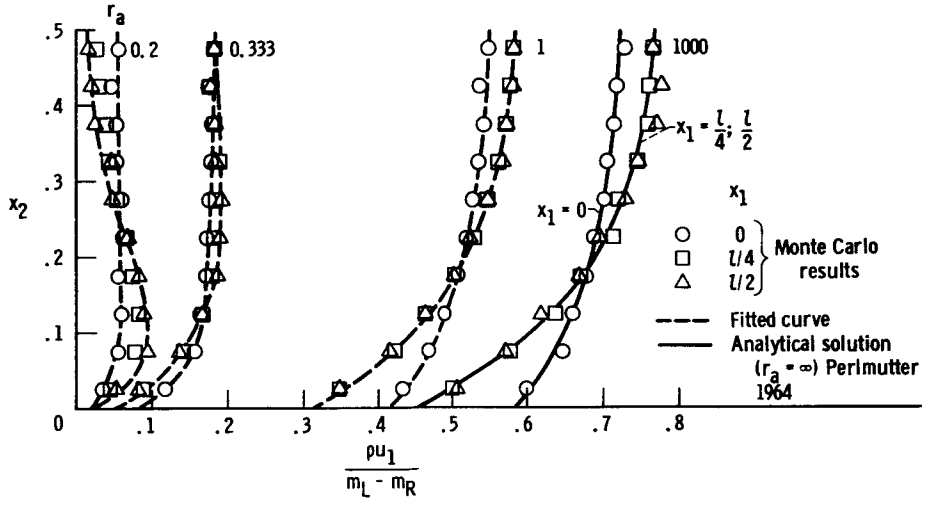

(b) Channel length divided by height, $l = 1.0$.

Figure 3. - Continued. Axial mass flow profiles.

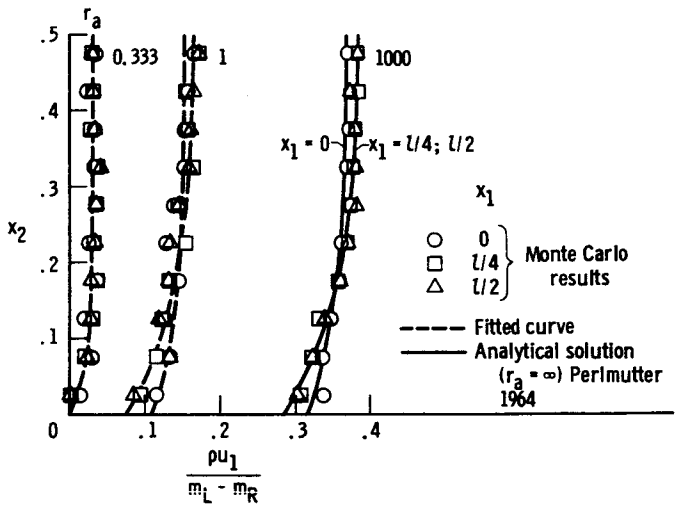

(c) Channel length divided by height, $l = 5$.

Figure 3. - Concluded. Axial mass flow profile.

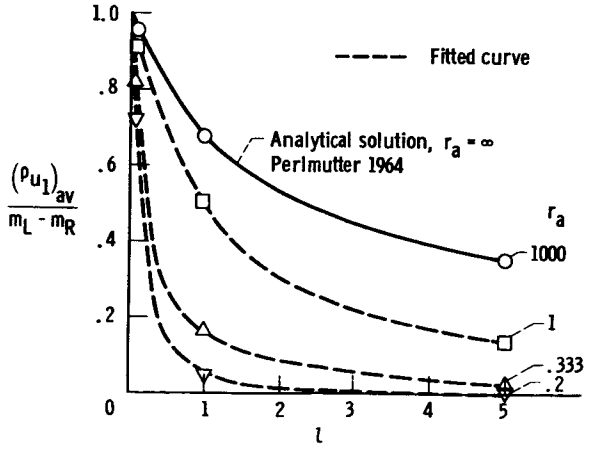

Figure 4. - Average mass flow through channel.

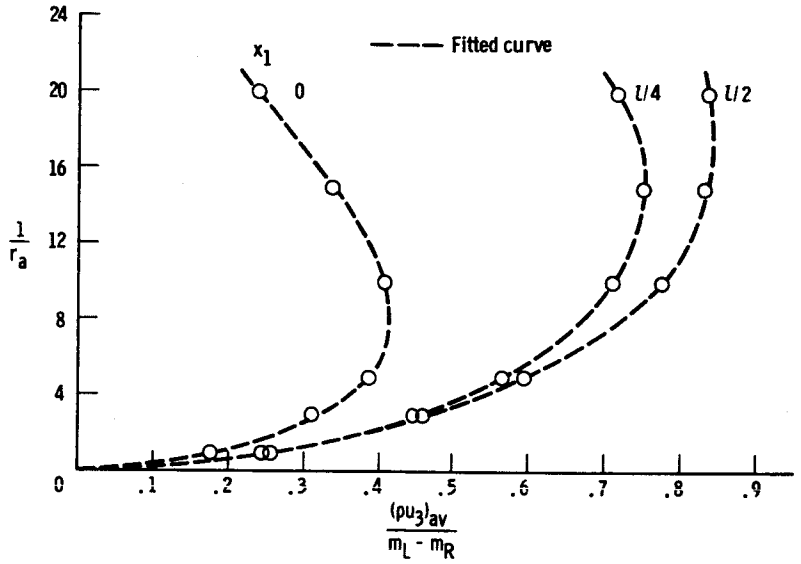

(a) Channel length divided by height, $l = 0.1$.

Figure 5. - Average transverse flow across channel.

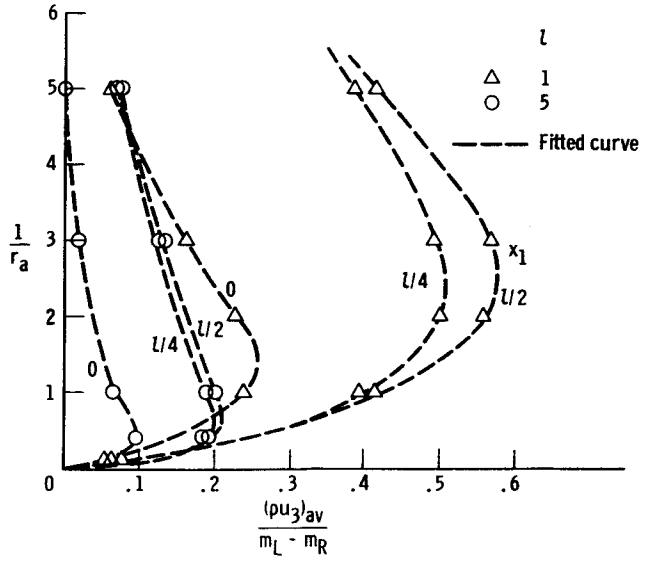

(b) Channel length divided by height, $l = 1.0$ and 5.

Figure 5. - Concluded. - Transverse flow across channel.

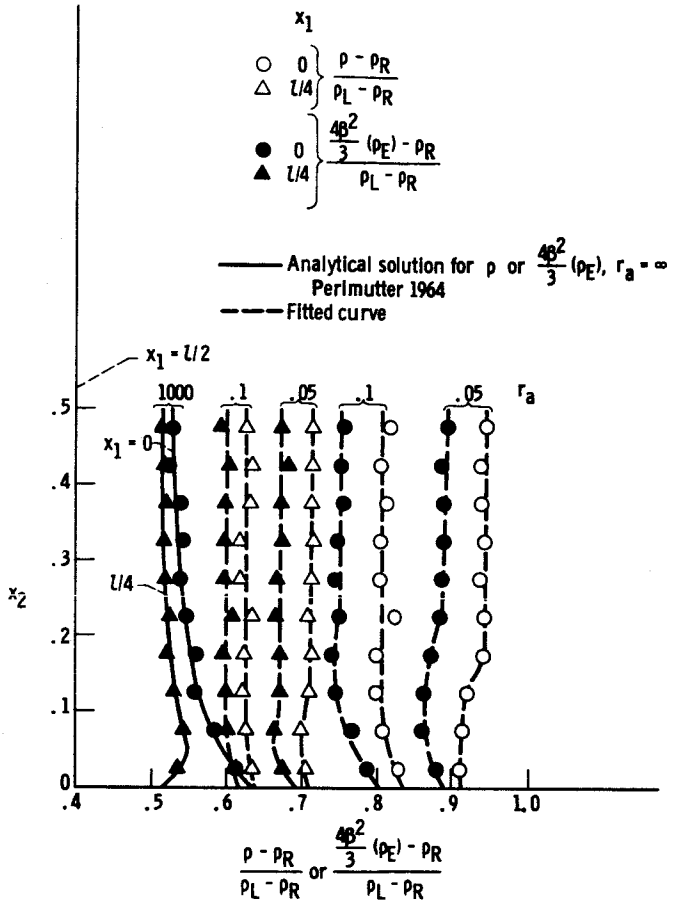

(a) Channel length divided by height, $l = 0.1$.

Figure 6. - Density and energy distributions in channel.

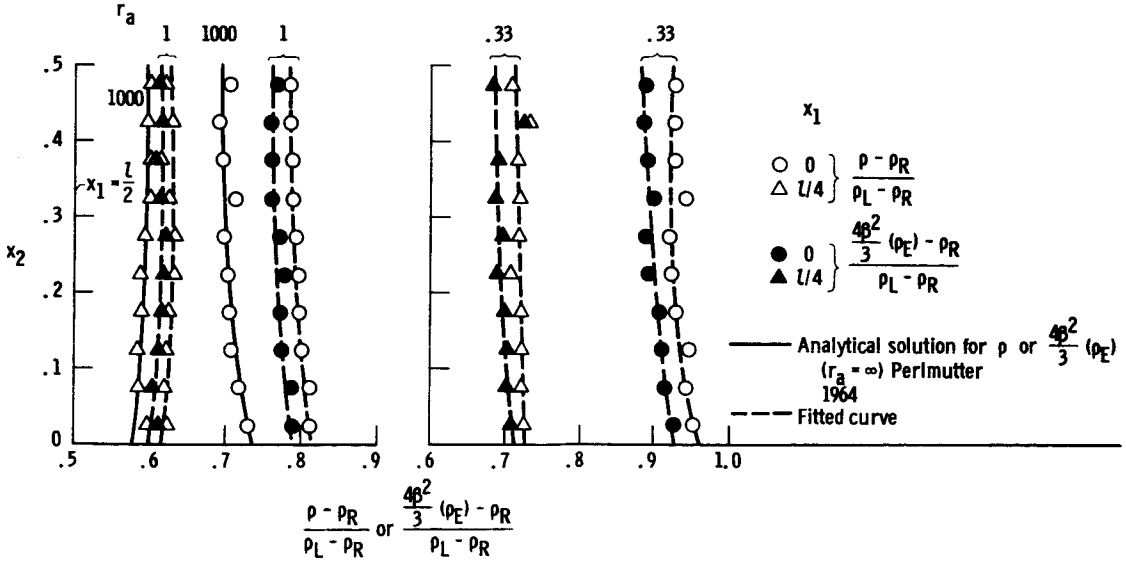

(b) Channel length divided by height, $l = 1.0$.

Figure 6. - Concluded. Density and energy distributions in channel.

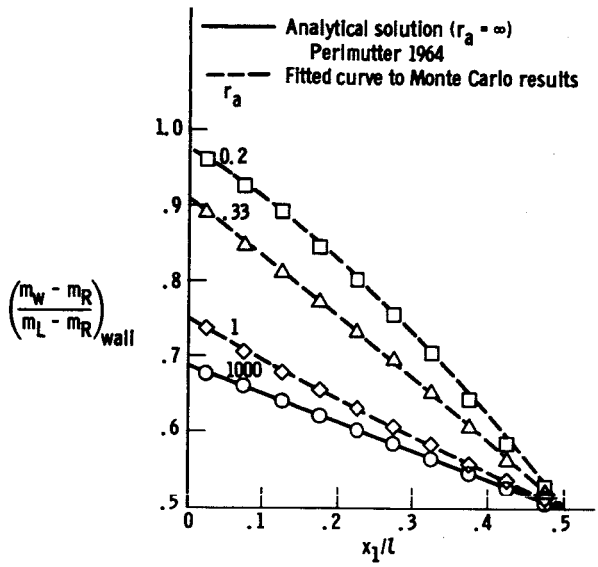

(a) Channel length divided by height, $l = 1.0$.

Figure 7. - Mass flow reflected from wall.

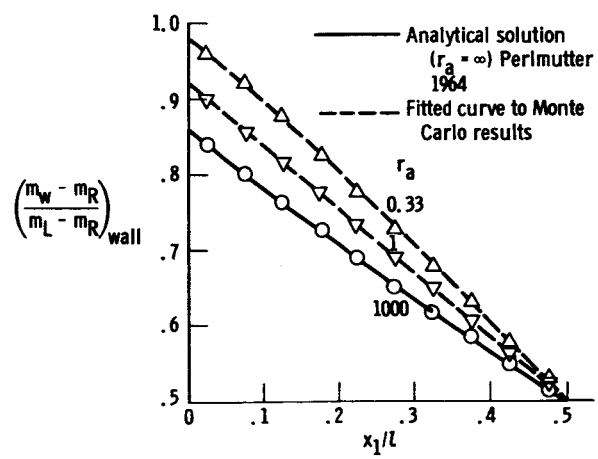

(b) Channel length divided by height, $l = 5$.

Figure 7. - Concluded. Mass flow reflected from wall.

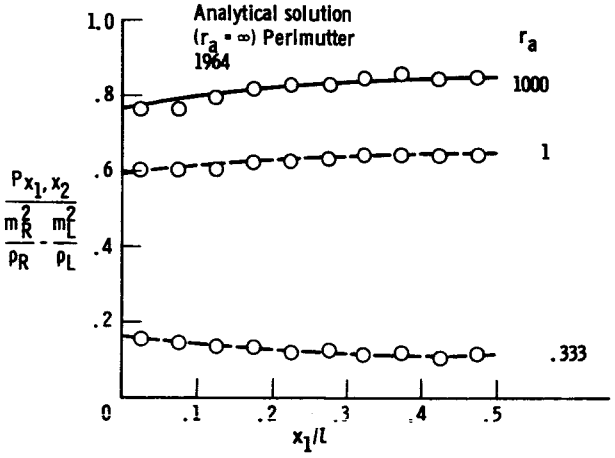

Figure 8. - Wall shear distribution. Channel length divided by height, $l = 1.0$.

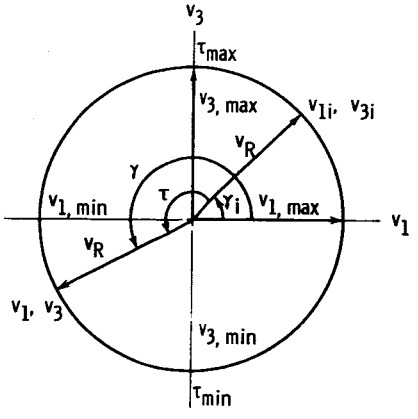

Figure 9. - Velocity relations.